
Structure, synthesis and characterization of contrast agents for magnetic resonance molecular imaging

Sophie Laurent, Luce Vander Elst, Alain Roch, Robert N. Muller

Department of General, Organic and Biomedical Chemistry, NMR and Molecular Imaging Laboratory, University of Mons-Hainaut, B-7000 Mons, Belgium
robert.muller@umh.ac.be

1 Introduction

Magnetic resonance imaging (MRI) is a non invasive method that, in a medical context, allows the identification and characterization of pathological tissues and lesions. The principle of this technique is based on the application of magnetic field gradients in three dimensions. The image results from the spatial identification of hydrogen nuclei. This image is constituted of elements, “pixels”, where grey levels represent the signal intensity emitted by corresponding volume elements, “voxels”. As the signal depends on the concentration in protons and on nuclear relaxation times, T_1 and T_2 , modulations of image intensity are observed.

To make a precise medical diagnosis, contrast agents facilitating the distinction between pathological and healthy tissue are administered. Their role is to modify the nuclear density and nuclear relaxation times. Instrumental parameters such as the choice of the sequence can also influence the contrast. Among the characteristics of these substances, the efficiency and safety for the patient must be determined before considering medical application. The contrast agents therefore have to be stable, non toxic, biocompatible and efficient at weak doses.

The intensities on MRI image are mainly determined by water proton relaxation. The process of relaxation is a function of the water proton environment and varies according to the tissues. The contrast can be modulated by two phenomena governing the relaxation of protons: the T_1 effect or longitudinal relaxation, which increases the signal intensity (positive agent), or the T_2 effect or transverse relaxation, which decreases the signal intensity (negative agent). Images will then be weighted in T_1 or T_2 .

2 Contrast agents

To increase the signal intensity and image quality, contrast agents are used [1,2,3] (fig. 1). Their key property is their "relaxivity", defined as the aptitude to increase the water proton relaxation rate by one mmol l^{-1} of paramagnetic center. These substances play the role of a real catalyst in relaxation and are classified into 3 categories according to their magnetism: diamagnetic, paramagnetic or superparamagnetic compounds. Contrast agents decrease the proton relaxation time and, thus, reduce the acquisition time of the image. More of the signal can be accumulated, which increases the sensitivity and the image contrast.

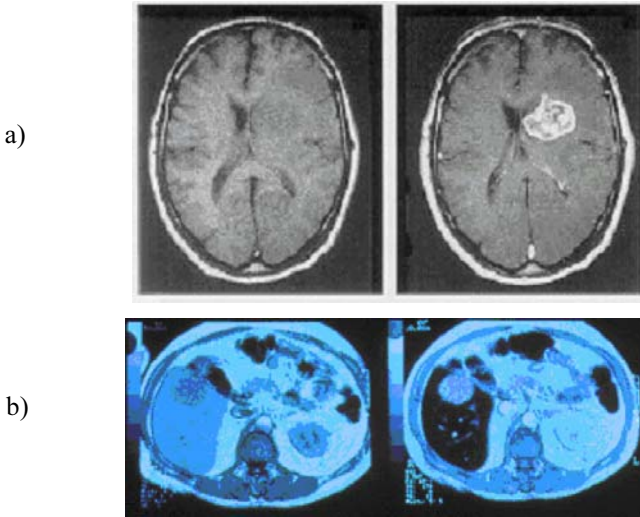


Fig. 1. MRI before injection of the contrast agent and after injection with the positive contrast agent (a) [4] and with a negative contrast agent (b).

Diamagnetic materials have a weak negative susceptibility in an external magnetic field. Their effect on signals is very weak.

Paramagnetic compounds include oxygen, nitroxides, transition metal ions and lanthanides. They possess one or several free electrons responsible for the presence of a dipolar magnetic field during the application of an external field B_0 . This magnetic moment is 657 times higher than that of the proton, and the paramagnetic effect is therefore superior to the diamagnetic effect. Gadolinium is a very toxic metal in the hydrated form $[\text{Gd}(\text{H}_2\text{O})_8]^{3+}$. To avoid toxicity while maintaining the magnetic and electronic properties of this ion, paramagnetic gadolinium complexes have been used. In vivo, the free Gd is in competition with calcium-dependent systems and blocks the reticulo-endothelial system. To avoid all in-vivo toxicity, it has to be used

in the form of a thermodynamically stable inert complex. Further, the ligand which complexes the metal has to leave free coordination sites such that one or several molecules of water can link to the metal, thus increasing the relaxivity. The first gadolinium complexes commercially available were Magnevist® (Gd-DTPA) and Dotarem® (Gd-DOTA). These compounds are accompanied by counter-ions that increase the osmolality of the injected solution. Two other “neutral” complexes exist, Omniscan® (Gd-DTPA-BMA) and Prohance® (Gd-HP-DO3A) [5]. These 4 paramagnetic complexes (fig. 2) disseminate freely in the extracellular space and present no specificity.

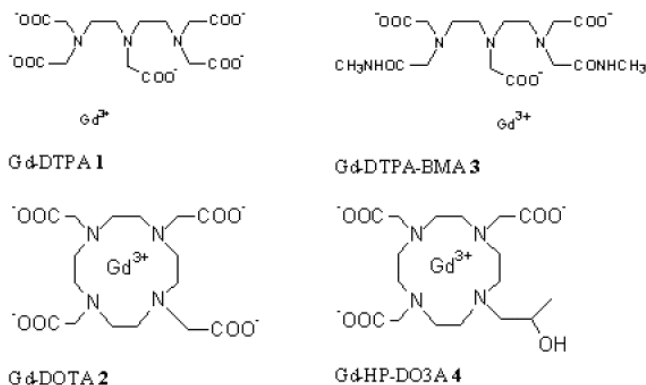


Fig. 2. Structure of commercial paramagnetic contrast agents.

The addition of lipophilic groups onto the skeleton of Gd-DTPA has improved the tissular tropism. When these derivatives accumulate at the level of some pathological tissues, they can greatly increase the signal intensity. Eovist® (Gd-EOB-DTPA), for example, targets hepatocytes (fig. 3). Another strategy is to covalently couple these gadolinium complexes to macromolecules such as human seric albumin (HSA) and polysaccharides (dextran), or to synthetic polymers such as polylysine, polyethyleneglycol, dendrimers, etc. An alternative for bettering the efficiency of contrast agents is the non-covalent interaction with HSA. Aryl moieties are grafted onto the contrast agent, which are able to recognize the hydrophobic sites of the protein.

The recent development in contrast agent research is the targeting of a sickness or its manifestations, for example the early detection of tumors. This strategy is based on the principle of recognition of specific receptors. Their ligands, i.e. peptides, antibodies, folate, . . . are grafted onto Gd-DTPA. Another class of smart agents modulates their efficiency according to the biological environment (the presence of enzymes, pO_2 , pH, and so on). For example, pH-sensitive agents are promising for pathologies that acidify the environment (in tumors, the pH is ~ 6.8 , while in a healthy extracellular medium, the

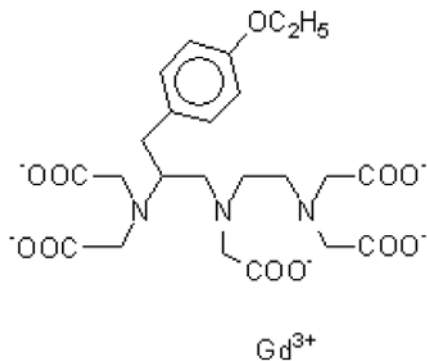


Fig. 3. Structure of Gd-EOB-DTPA.

pH is ~ 7.4).

Contrast compounds for angiography are notably characterized by prolonged vascular remanence time, decreased extravasation, biological inertia, efficient elimination, etc. To increase the vascular residence time, various strategies have been tried: imitating sanguine cellular structures (liposomes, micelles) or increasing the molecular mass by covalent bond to the macromolecules. However, these approaches have disadvantages that limit their application because, among other problems, they leave the bloodstream rapidly. Thus, the liposomes accumulate in the liver and spleen, the plasma protein mimetics are opsonized and recognized by the reticulo-endothelial system. A new strategy consists in grafting molecules of glucose onto the Gd-DTPA. Prolongation of the half-life of glucosylated Gd-DTPA derivatives is hypothesized to be due to a possible interaction with the renal glucose carrier, which can entail delayed renal excretion.

The last category is that of superparamagnetic nanoparticles (fig. 4), which are composed of an iron oxide nucleus of 5 nm diameter (SPIO, SuperParamagnetic Iron Oxide). To increase their stability in aqueous medium, particles are coated with polymers (dextran) and form colloidal solutions. The diameter of these particles is on the order of 10 - 20 nm. After intravenous injection, particles are trapped by cells of the reticulo-endothelial system (i.e. Kupffer cells in the liver, the spleen). They induce a diminution of the signal in these organs and are used for hepatic tumor detection. Current experiments aim to graft these contrast agents onto different molecules that target specific cellular receptors of a given pathology. MRI applications for these superparamagnetic compounds are quite various and go from angiography to tumoral diagnosis and atherosclerotic pathology. The progress of molecular biology in recent years has led to the development of new, increasingly specific methods of diagnostic imaging. Among these, molecular imaging has burgeoned thanks to the utilization of the magnetic marker and to a better spatial resolution. The

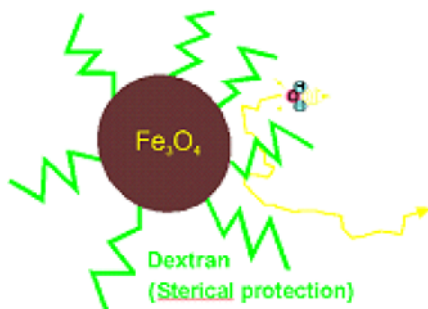


Fig. 4. Structure of iron oxide nanoparticles.

recent studies on cellular labeling in MRI have used the specific targeting of some cellular receptors with ligands grafted to SPIO (superparamagnetic iron oxide) or USPIO (ultrasmall superparamagnetic iron oxide) particles.

The most common method for producing magnetic nanoparticles involves coprecipitation of ferrous and ferric salts in an alkaline medium. This synthesis approach can be used in the absence or presence of surface complexing agents, such as PEG, dextran, synthetic polymer, to name a few. For the method without surface complexing agents, the nanoparticles precipitated are isolated through magnetic decantation or centrifugation. The precipitate is then treated with nitric acid, centrifuged and peptized in water to produce a stable acidic magnetic sol. Alkaline magnetic sols can be obtained using tetramethylammonium. A variety of factors can be adjusted in the synthesis protocol of the iron oxide particles in order to control size, magnetic characteristics, stability in solution or surface properties. Although coprecipitation methods are used for their simplicity, the nanoparticles produced are fairly polydisperse. Consequently, several other techniques are currently being developed to obtain nanoparticles with more uniform dimensions.

3 Relaxation mechanisms

3.1 Nuclear relaxation

Nuclear relaxation corresponds to the return to thermodynamic equilibrium of a spin system excited by the energy absorbed during the application of an electromagnetic field of appropriate frequency.

The interaction of magnetic moments of the excited spins with the environment creates fluctuating local microscopic magnetic fields. These magnetic

fluctuations are linked to molecular movement. Longitudinal (R_1) and transverse (R_2) relaxation rates are therefore modulated by the phenomenon of molecular distribution and are expressed by the generic relationship:

$$\frac{1}{T_i} = R_i = KE_c^2 f(\tau_c) \quad (1)$$

where:

$i = 1, 2$

K is a constant

E_c is the amplitude of the interaction responsible for the relaxation

$f(\tau_c)$ is a function of the correlation time, τ_c , that modulates the interaction.

3.2 Paramagnetic relaxation

The presence of paramagnetic ions entails the increase of the observed relaxation rate of water protons. This equation can be written as:

$$\frac{1}{T_i^{obs}} = \frac{1}{T_i^{dia}} + \frac{1}{T_i^p} \quad (2)$$

where $1/T_i^{dia}$ is the diamagnetic relaxation rate of water protons without paramagnetic contribution and $1/T_i^p$ is the paramagnetic relaxation rate.

The paramagnetic center influences the relaxation rate of the water molecule which interacts directly with it and the neighboring molecules.

The efficiency of contrast compounds is linked to molecular movements but also to intrinsic properties of the nuclei (magnetic moment, gyromagnetic ratio, spin). The paramagnetic relaxation R_1^p is characterized by two contributions: the contribution of internal sphere R_1^{is} ("inner sphere", IS, fig. 5) and external sphere R_1^{os} ("outer sphere", OS, fig. 6). The principle of "inner sphere" relaxation is a chemical exchange during which one or several water molecules are in contact with the electronic spin; after leaving the first sphere of coordination of the paramagnetic center, they are replaced by other molecules. This mechanism allows the propagation of the paramagnetic effect to the totality of the solvent and constitutes a situation where the water molecule is exchanged between two sites (the interior and the exterior of the first coordination sphere). The IS model has been described by the Solomon-Bloembergen-Morgan theory (SBM) [6, 7].

The inner sphere contribution is given by:

$$R_1^{is} = fq \frac{1}{T_{1M} + \tau_M} \quad (3)$$

$$\frac{1}{T_{1M}} = \frac{2}{15} \left(\frac{\mu_0}{4\pi} \right)^2 \gamma_H^2 \gamma_S^2 \hbar^2 S(S+1) \frac{1}{r^6} \left[\frac{7\tau_{c2}}{1 + (\omega_S \tau_{c2})^2} + \frac{3\tau_{c1}}{1 + (\omega_H \tau_{c1})^2} \right] \quad (4)$$

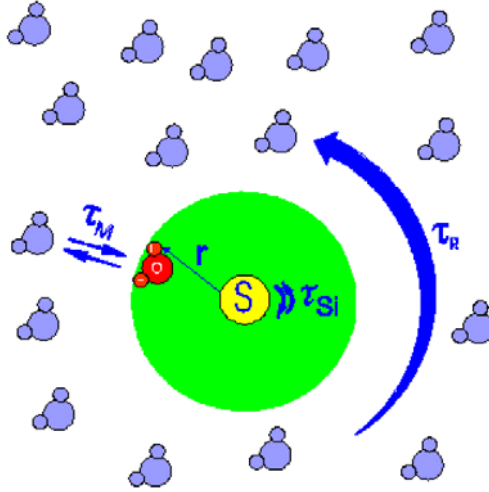


Fig. 5. Schematic representation of the inner sphere theory (IS).

$$\frac{1}{\tau_{ci}} = \frac{1}{\tau_R} + \frac{1}{\tau_M} + \frac{1}{\tau_{si}} \quad (5)$$

$$\frac{1}{\tau_{S1}} = \frac{1}{5\tau_{SO}} \left[\frac{1}{1 + \omega_S^2 \tau_V^2} + \frac{4}{1 + 4\omega_S^2 \tau_V^2} \right] \quad (6)$$

$$\frac{1}{\tau_{S2}} = \frac{1}{10\tau_{SO}} \left[3 + \frac{5}{1 + \omega_S^2 \tau_V^2} + \frac{2}{1 + 4\omega_S^2 \tau_V^2} \right] \quad (7)$$

where f is the relative concentration of the paramagnetic complex and of the water molecules; q is the number of water molecules in the first coordination sphere; τ_M is the water residence time; γ_S and γ_H are the gyromagnetic ratios of the electron (S) and of the proton (H), respectively; $\omega_{S,H}$ are the angular frequencies of the electron and of the proton; r is the distance between coordinated water protons and the unpaired electron spin; $\tau_{c1,2}$, the correlation times modulating the interaction, are defined by Eq. 5 – where τ_R is the rotational correlation time of the hydrated complex and $\tau_{s1,2}$ are the longitudinal and transverse relaxation times of the electron. These latter parameters are field-dependent (Eqs. 6 and 7). τ_{SO} is the value of $\tau_{s1,2}$ at zero field and τ_v is the correlation time characteristic of the electronic relaxation times.

The second contribution to paramagnetic relaxation is "outer sphere" relaxation. It is explained by the dipolar interaction at long-distance between the spin of the paramagnetic substance and the nuclear spin. This intramolecular mechanism is modulated by the translational correlation time (τ_D) that takes into account the relative molecular diffusion constant (D) between the paramagnetic center and the solvent molecule, as well as their distance of closest approach (d). The OS model has been described by Freed [8].

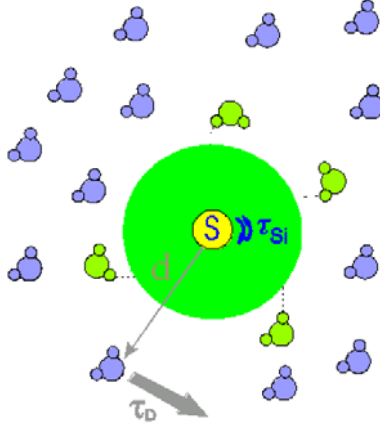


Fig. 6. Schematic representation of outer sphere theory (OS).

The outer sphere contribution is given by:

$$R_1^{os} = \frac{6400\pi}{81} \left(\frac{\mu_0}{4\pi}\right)^2 \gamma_H^2 \gamma_S^2 \hbar^2 S(S+1) N A \frac{[C]}{dD} [7j(\omega_S \tau_D) + 3j(\omega_H \tau_D)] \quad (8)$$

$$j(\omega \tau_D) = Re \left[\frac{1 + \frac{1}{4} \left(i\omega \tau_D + \frac{\tau_D}{\tau_{S1}} \right)^{1/2}}{1 + \left(i\omega \tau_D + \frac{\tau_D}{\tau_{S1}} \right)^{1/2} + \frac{4}{9} \left(i\omega \tau_D + \frac{\tau_D}{\tau_{S1}} \right) + \frac{1}{9} \left(i\omega \tau_D + \frac{\tau_D}{\tau_{S1}} \right)^{3/2}} \right] \quad (9)$$

[C] is the molar concentration of the paramagnetic ion and $\tau_D = d^2/D$ is the translational correlation time.

4 Physico-chemical characterization of contrast agents

4.1 Paramagnetic complexes

The complexity of the equations describing the relaxation rate justifies the large number of parameters describing the relaxation IS and OS (8 parameters: τ_M , q , τ_R , D , r , d , τ_V , τ_{S0}). Considering the high number of parameters introduced by the equations, the estimation of all parameters using the technique of field cycling is often ambiguous. Thus, the determination of some parameters using independent methods increases the overall reliability of the theoretical adjustment of the NMRD curve (fig. 7) [9, 10, 11, 12, 13].

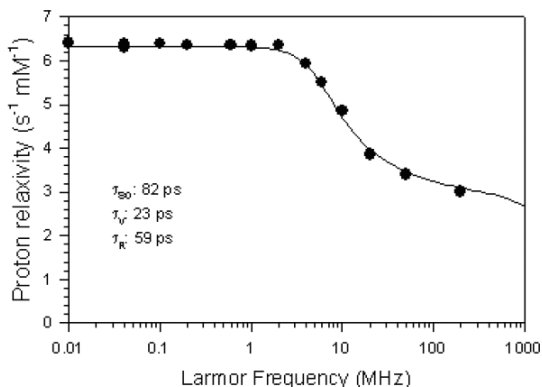


Fig. 7. NMRD profile of Gd-DTPA.

Rotational correlation time

The rotational correlation time (τ_R) characterizes the reorientation of the spin-nucleus vector, such as the Gd^{3+} -proton vector of the water molecule in the case of a gadolinium complex. Generally, τ_R limits the complex relaxivity of low molecular weight complexes in the fields range used in imaging. This characteristic can be exploited advantageously. The rotational correlation time can be obtained through several methods: analysis of the longitudinal relaxation of ^{17}O on the Gd complex, EPR measurement of the vanadyl complex, measurement of the longitudinal relaxation rate by ^{13}C NMR, fluorescence polarization spectroscopy or by deuterium relaxation rate.

In small diamagnetic molecules, the longitudinal relaxation rate of deuterium nuclei is given by equation 10, where the quantity in brackets is the quadrupolar coupling constant ($e^2qQ/h = 170$ kHz for D-C_{sp^3}).

$$R_1 = \frac{1}{T_1} = \frac{3}{8} \left(\frac{e^2qQ}{\hbar} \right)^2 \tau_R \quad (10)$$

Electronic relaxation times

Longitudinal and transversal electronic relaxation times (τ_{S1} and τ_{S2}) describe the process of return to equilibrium of the magnetization associated with electrons undergoing transitions between the electronic levels of the Gd ion. These transitions produce fluctuations that enable the relaxation of protons. The degeneration of the higher electronic level of gadolinium ions occupied by single electrons is attributed to the Zeeman effect. It seems that the origin of electronic transition is represented by the collisions between solvent

molecules and the complex that induces distortions in symmetry and leads to transitory ZFS of electronic levels.

Electronic relaxation rates depend on the field. In the case of Gd complexes, electronic relaxation rates are quite long ($\sim 10^{-10}$ s at low field and $\sim 10^{-8}$ - 10^{-7} s at high field). Consequently, the influence of electronic relaxation is especially evident at fields inferior to 0.2 Tesla.

Number of water molecules coordinated to metal

The number of water molecules strongly influences the IS contribution because the relation is directly proportional. For complexes like Gd-DTPA, an increase in the number of water molecules from 1 to 2 enhances relaxivity by about 30%, but nearly all derivatives of Gd-DTPA are $q=1$. Two types of measurements can be distinguished: q in solid phase and q in solution. Measurements in solid phase are obtained by diffraction (X rays, neutron diffraction). Although there is generally a good correlation between measurements obtained in these two different states of matter, by definition, measurement in solid phase does not take into account the dynamic state of the complex. It is therefore useful to confirm these measurements by doing studies in solution. The fluorescence of Eu or Tb complexes can be induced by laser. The disexcitation rate by fluorescence of the two lanthanides follows an exponential decrease and is proportional to the number of water molecules coordinated to the metal. This disexcitation rate differs according to whether the complexes are coordinated to H_2O or D_2O . The measurement in these two media and their subtraction allows the calculation of number q . Another possibility is the LIS (Lanthanide Induced Shift) method that makes it possible to determine the number of water molecules coordinated by ^{17}O NMR.

Proton-to-metal distance

For protonic relaxation in the presence of paramagnetic centers, the IS contribution is manifested by dipolar interactions. The efficiency of the dipolar mechanism comprises the term in $1/r^6$, where r is the metal-to-proton distance. One understands therefore that even a slight reduction in this distance will have a noticeable impact on the relaxivity of Gd-DTPA complex.

This reduction could be the cause of the higher relaxivity of Gd-EOB-DTPA ($5.5 \text{ mM}^{-1} \text{ s}^{-1}$ at 310 K, 20 MHz) with respect to Gd-DTPA ($3.9 \text{ mM}^{-1} \text{ s}^{-1}$ at 310 K, 20 MHz). While the exact distance between the gadolinium and the oxygen in water is well defined thanks to crystallographic structures, the Gd-water-proton distance is only an estimate because few experimental methods allow this measurement.

Coordinated water exchange rate

The mechanism of IS relaxation is based on an exchange between water molecules surrounding the complex and the water molecule(s) coordinated

to the lanthanide. Consequently, for agents of paramagnetic relaxation, the exchange rate ($k_{ex} = 1/\tau_M$) is an essential parameter for the transmission of the "relaxing" effect to the solvent surrounding the complex. The principle of measurement is based on Swift and Connick's works on diluted paramagnetic solutions. It consists of analyzing the transverse relaxation rate of ^{17}O as a function of the temperature.

The paramagnetic transverse relaxation rate of water in solutions of gadolinium complexes is given by equation 11 where T_{2M} , the transverse relaxation rate of the oxygen atom of the bound water, results from scalar interaction between the electron and the oxygen nucleus (Eq. 12) and $\Delta\omega_M$, the chemical shift of the oxygen in this water molecule is given by Eq. 13. The outer sphere contribution is neglected.

$$\frac{1}{T_2^{is}} = f q \frac{1}{\tau_M} \frac{\frac{1}{T_{2M}^2} + \frac{1}{\tau_M T_{2M}} + \Delta\omega_M^2}{\left(\frac{1}{\tau_M} + \frac{1}{T_{2M}}\right)^2 + \Delta\omega_M^2} \quad (11)$$

$$\frac{1}{T_{2M}} = \frac{1}{3} S(S+1) \left(\frac{A}{\hbar}\right)^2 \left[\tau_{e1} + \frac{\tau_{e2}}{1 + \omega_S^2 \tau_{e2}^2} \right] \quad (12)$$

$$\Delta\omega_M = \frac{g_L \mu_B S(S+1) B_o}{3k_B T} \frac{A}{\hbar} \quad (13)$$

A/\hbar is the hyperfine or scalar coupling constant between oxygen and Gd^{3+} ; τ_{ei} are given by $[\tau_M^{-1} + \tau_{Si}^{-1}]^{-1}$; g_L , the Landé factor, is equal to 2.0 for Gd^{3+} ; μ_B is the Bohr magneton; B_0 is the external magnetic field.

The temperature dependence of τ_M and τ_V can be described by Eqs. 14 and 15, respectively.

$$\frac{1}{\tau_M} = \frac{k_B T}{\hbar} \exp\left(\frac{\Delta S^\ddagger}{R} - \frac{\Delta H^\ddagger}{RT}\right) \quad (14)$$

$$\tau_V = \tau_V^{298} \exp\left(\frac{E_v}{R} \left(\frac{1}{T} - \frac{1}{298.15}\right)\right) \quad (15)$$

ΔS^\ddagger and ΔH^\ddagger are the entropy and the enthalpy of activation for the exchange process, τ_V^{298} is the correlation time at 298.15 K and E_v is the activation energy for this process.

4.2 Superparamagnetic nanoparticles

Proton relaxation in superparamagnetic colloids occurs because of the fluctuations of dipolar magnetic coupling between nanocrystal magnetization and proton spin. The relaxation is described by an outer sphere model where the dipolar interaction fluctuates because of both the translational diffusion process and the Néel relaxation process.

The simplest model [14] is derived when the anisotropy energy of the crystal is great enough to prevent any precession of its magnetic moment. In this high anisotropy condition, the magnetization of the crystal is locked along the easy axes. The magnetic fluctuations then arise from the jumps of the moment between different easy directions according to the Néel relaxation process.

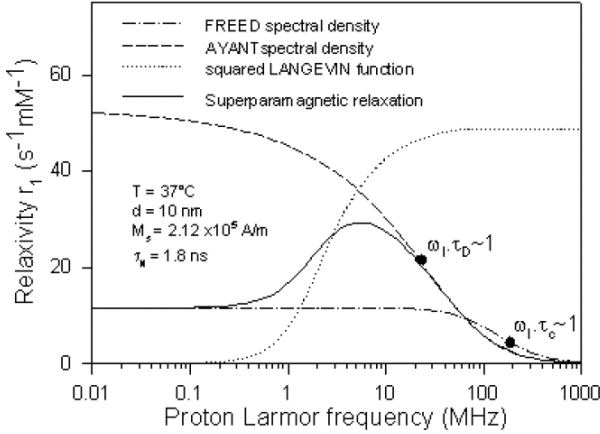


Fig. 8. Illustration of the superparamagnetic model.

At low fields (Fig. 8), the longitudinal relaxation rate of the protons is obtained by introducing in the outer sphere equations the limitation of the precession as mentioned above: the electron Larmor precession frequency is set to zero. The spectral density function determining this component of the relaxation is then characterized by a global correlation time depending on τ_N and τ_D . τ_N and τ_D are respectively the Néel relaxation time and the translation correlation time. Figure 8 shows the dispersion of this spectral density function, called the Freed function.

For very small crystals, the assumption of a complete locking of the magnetization along the easy axes, assuming an infinite anisotropy energy, becomes less and less valid. Subsequently, the orientation of the magnetization vector out of the easy axes becomes more probable [15]. This results in the presence of low field dispersion (Fig. 9). The evaluation of the amplitude of the low field component requires a more complete and difficult theory that takes into account the anisotropy. Note that the low field dispersion is always smaller than that predicted by the classical paramagnetic outer sphere theory. Indeed, the classical theory would be valid only for superparamagnetic colloids characterized by a null anisotropy [16].

At high fields (Fig. 8), the magnetic vector is locked along the external field B_0 , and Curie relaxation dominates. The corresponding relaxation rates are

given by an outer sphere model assuming a stationary magnetization component in the B_o direction and, therefore, an infinite value of the Néel relaxation time. The dispersion of this spectral density (named the Ayant function) occurs when $\omega_I \cdot \tau_D \sim 1$.

At intermediate fields (Fig. 8), the relaxation rates are combinations of the high and low field contributions, weighted by factors depending on the Langevin function, which gives the average magnetization of the sample.

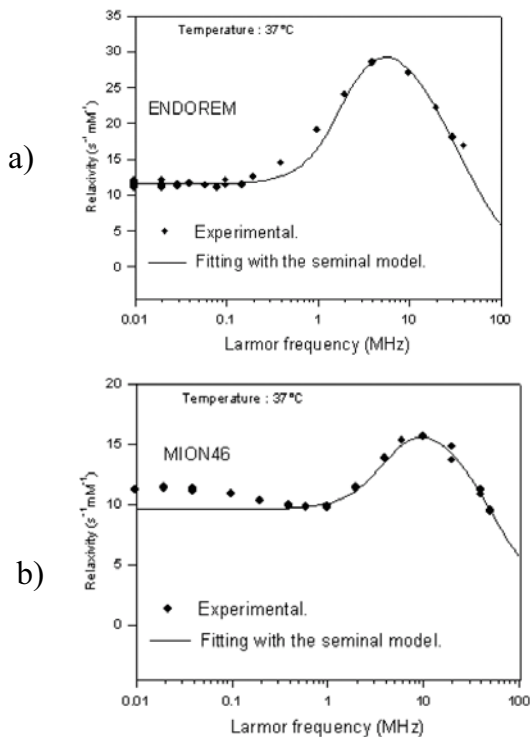


Fig. 9. Comparison between NMRD curves of particles with high (a) and low (b) anisotropy. As the anisotropy energy is proportional to the crystal volume, curve A corresponds to larger crystals.

The analysis of the proton NMRD profiles thus gives:

1. *the average radius (r):* at high magnetic fields, the relaxation rate depends only on τ_D and the inflection point corresponds to the condition $\omega_I \cdot \tau_D \sim 1$ (Fig. 10). As shown in Eq. 16, the determination of τ_D gives the crystal size r . r , D and ω_I are the average radius of the superparamagnetic crystals, the relative diffusion coefficient, and the proton Larmor pulsation, respectively.

$$\tau_D = \frac{r^2}{D} \tag{16}$$

2. *the specific magnetization (M_s):* at high fields, M_s can be obtained from the equation $M_s \sim C.(R_{max}/\tau_D)^{1/2}$, where C is a constant and R_{max} the maximal relaxation rate.

3. *the crystal anisotropy energy (E_a):* the absence or the presence of dispersion at low fields informs about the magnitude of the anisotropy energy. For crystals characterized by a high E_a value as compared to the thermal agitation, the low field dispersion disappears. This was confirmed in a previous work with cobalt ferrites [17], known to have high anisotropy energy.

4. *the Néel relaxation time (τ_N):* the relaxation rate at very low field R_0 is governed by a “zero magnetic field” correlation time τ_{C0} which is equal to τ_N if $\tau_N \ll \tau_D$. However, this situation is not met often, so τ_N is frequently reported as qualitative information additional to the crystal size and the specific magnetization.

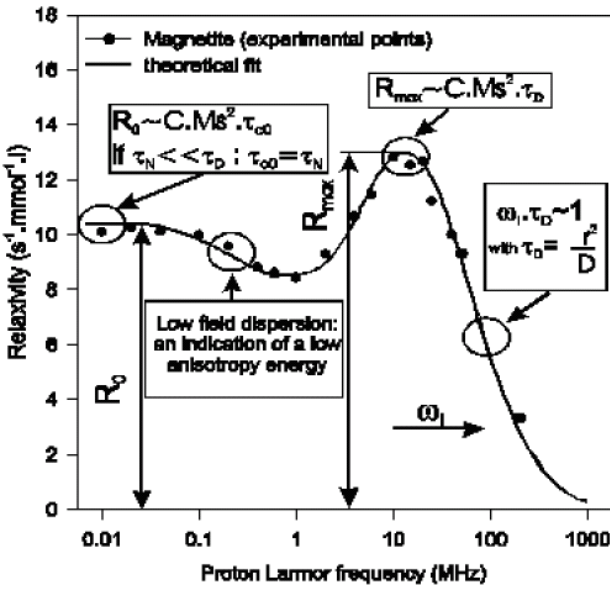


Fig. 10. NMRD profile of magnetite particles in colloidal solution.

5 Magnetic applications: MRI, cellular targeting

One possible way of extending the vascular residence time of contrast agents resides in the renal reabsorption mechanisms of some molecules such as glu-

cose. Thus, various small-molecular-weight glucosyl derivatives of gadolinium diethylenetriaminepentaacetic (Gd-DTPA) were synthesized and their vascular half-life was studied. The sugar moieties linked to Gd-DTPA efficiently reduce the renal excretion of some derivatives. The interaction with the renal carrier was not clearly demonstrated, nor was any interaction with blood components observed. New glucosylated derivatives of Gd-DTPA (Cd-DTPA-BC₂-beta-cellobionA and Gd-DTPA-BC₄-beta-glucosylA) have been proposed as blood-pool MR contrast agents, considering their vascular remanence [18].

Apoptosis is a physiological process that becomes pathologic either by overactivity or inhibition. A dedicated contrast agent evidencing pathologies where apoptosis takes place would be useful for monitoring antitumor therapies. Phage display is a powerful new method used to select peptides with high affinity for a given target - phosphatidylserine (PS) in this study. Subsequent coupling of the selected peptides with a magnetically active species produces selective MRI contrast agents. The efficacy of this new contrast agent was tested on cells in culture [19].

Targeting of the endothelial inflammatory adhesion molecule E-selectin by MRI can be performed with a paramagnetic or superparamagnetic contrast agent in the context of in vitro and in vivo models of inflammation [20, 21]. The specific contrast agent was obtained by grafting a synthetic mimetic of sialyl Lewis^x (sLe^x), a natural ligand of E-selectin expressed on leukocytes, on the DTPA-bisanhydride or on the dextran coating of ultrasmall particles of iron oxide (USPIO).

Bulté has used MRI to provide information on the location and migration of cells after transplantation or transfusion. This approach requires magnetic prelabeling of the cells. With the magnetic labeling methods currently available, it is anticipated that cellular MRI will find applications in biology and medicine [22].

Magnetic hyperthermia involves dispersing nanoparticles into the targeted tissue and then applying a magnetic field to heat the particles. This heat is conducted into the immediately surrounding diseased tissue. Hyperthermia treatment of cancers is based on the finding that some cancer cells are more sensitive to temperatures in excess of 41°C than are their normal healthy counterparts [23, 24]. Magnetic nanoparticles encapsulated in polymer matrix beads have been used successfully for the treatment of macroscopic liver tumor.

Conclusions

MRI plays an important role in modern medicine and is at the interface of several scientific domains such as chemistry, biology and the physical sciences. Superparamagnetic particles present a lot of advantages in terms of molecular imaging because: (i) they constitute very powerful transverse relaxophores

and therefore are very efficient for use as a negative contrast agent. (ii) superparamagnetic crystals allow the fixation of several thousand active iron atoms, instead of only one in the case of paramagnetic complexes, to a single cell receptor. (iii) iron oxide particles are absolutely non toxic and bio-compatible. (iv) as shown in this review, there are many ways to graft the molecular entities that are the most suitable for targeting the desirable receptor. (v) the new means of synthesis recently discovered would optimize the size distribution of the crystal and thus the performance of the contrastophore. The challenge for chemists is, hence, to increase the relaxivity of their "contrastophores".

References

1. P. Caravan, J.J. Ellison, T.J. Mc Murry, R.B. Lauffer, *Chem.Rev.* 99, 2293 (1999)
2. P.A. Rinck in *Magnetic Resonance in Medicine*, 4th edition, (Blackwell Wissenschafts, Verlag, Berlin-Vienna, 2001)
3. R.N. Muller, in *Contrast Agents in whole body MR: operating mechanisms*, Encyclopedia of NMR, (Wiley, New-York (1996)) p. 1438
4. A. Alaux, in *L'imagerie par Résonance Magnétique* (Éditions Sauramp Médical, 1994)
5. S. Laurent, L. Vander Elst, R.N. Muller, *Contrast Med. Mol. Imaging*, 1(3), 128 (2006)
6. I. Solomon, *Phys. Rev.* 99, 559 (1955)
7. N.J. Bloembergen, *Chem. Phys.* 27, 572 (1957)
8. J.H. Freed, *J. Chem. Phys.* 68, 4034 (1978)
9. L. Vander Elst, F. Maton, S. Laurent, F. Seghi, F. Chapelle, R.N. Muller, *Magn. Reson. Med.* 38, 604 (1997)
10. R.N. Muller, B. Raduchel, S. Laurent, J. Platzek, C. Piérart, P. Mareski, L. Vander Elst, *Eur. J. Inorg. Chem.* 1949 (1999);
11. S. Laurent, L. Vander Elst, S. Houzé, N. Guérit, R.N. Muller, *Helv. Chim. Acta* 83, 394 (2000)
12. S. Laurent, F. Botteman, L. Vander Elst, R.N. Muller, *Magn. Reson. Mater. Phys. Biol. Med.* 16(5), 235 (2004)
13. S. Laurent, F. Botteman, L. Vander Elst, R.N. Muller, *Helv Chem Acta* 87, 1077 (2004)
14. A. Roch, R.N. Muller in *Longitudinal relaxation of water protons in colloidal suspensions of superparamagnetic crystals* Proceedings of the 11th Annual Meeting of the Society of Magnetic Resonance in Medicine 11, 1447 (1992).
15. A. Roch, R.N. Muller, P. Gillis, *J Chem Phys.* 110, 5403 (1999).
16. A. Roch, R.N. Muller, P. Gillis, *J Magn Reson Imaging* 14, 94 (2001).
17. A. Roch, P. Gillis, A. Ouakssim, R.N. Muller, *J Magn Magn Mater.* 201, 77 (1999)
18. C. Burtea, S. Laurent, J-M. Colet, L. Vander Elst, R.N. Muller, *Invest. Radiol.* 38(6), 320 (2003)
19. C. Laumonier, J. Segers, S. Laurent, A. Michel, F. Coppée, A. Belayew, L. Vander Elst, R.N. Muller, *J. Biomol. Screening* 11(5), 537 (2006)

20. S. Boutry, C. Burtea, S. Laurent, L. Vander Elst, R. Muller, *Magn. Reson. Med.* 53(4), 800 (2005)
21. S. Boutry, S. Laurent, L. Vander Elst, R.N. Muller, *Contrast Med. Mol. Imaging* 1(1), 15 (2006)
22. J.W. Bulté, *Methods Mol. Med.* 124, 419 (2006)
23. A. Jordan, R. Scholz, P. Wust, H. Föhling, R. Felix, J. Magn. Mater. 210, 413 (1999)
24. P. Moroz, S.K. Jones, C. Metcalf, B.N. Gray, *Int. J. Hyperthermia* 19, 23 (2003)

See also the following WebSites:

- <http://www.umh.ac.be/~nmrlab/>
- <http://www.ami-imaging.org>
- <http://www.molecularimaging.org>
- <http://www.emrf.org>
- <http://www.ismrm.com>
- <http://www.esmrm.com>
- <https://matar.ciril.fr/JSTIM/>